IEEE/ASME Transactions on Mechatronics, 2012, Volume: PP , Issue: 99, Pages 1 - 10

Design and Simulation of a Novel Bio-Mechanic Piezoresistive Sensor with Silicon Nanowires

M. Messina, J. Njuguna, *School of Applied Sciences, Cranfield University, UK*

V. Dariol, C. Pace, G. Angeletti*, EM Motorsport, UK*

Abstract—**This paper presents the design of a novel single square millimeter 3-axial accelerometer for head injury detection of racing car drivers. The main requirements of this application are miniaturization and high-G measurement range.**

We propose a new miniature accelerometer to be incorporated into an earpiece. Nanowires as nanoscale piezoresistive devices have been chosen as sensing element, due to their high sensitivity and miniaturization achievable. By exploiting the electro-mechanical features of nanowires as nanoscale piezoresistors, the nominal sensor sensitivity is overall boosted by more than 30 times. This approach allows significant higher accuracy and resolution with smaller sensing element in comparison with conventional devices without the need of signal amplification. This achievement opens up new developments in the area of implanted devices where the high-level of miniaturization and sensitivity is essential.

***Index Terms*—Accelerometer, biomedical devices, giant piezoresistance, implantable sensors, silicon nanowires.**

I. INTRODUCTION

Si-based devices have dominated integrated circuit devices for many decades. Because silicon nanowires (SiNWs) can transport electrons and holes, with enhanced opto-electro-mechanical properties mainly due to

the quantum confinement effect, they could function as building blocks for nanoscale electronics and advanced devices [1]. Furthermore, nanowires have a very large piezoresistance effect [2]-[6], capable of enhancing the mechanical sensors performance, which is now actively being explored to improve silicon transistors [7], [8].Silicon nanowires are also attractive for applications in the filed-emission devices, photonics, chemical sensors and spintronics [9].

The piezoresistive effect is used for transducing, for example, acceleration in an electrical output. After an inertial force is applied to the sensor the strain on the piezoresistive material (silicon) changes its electrical resistance proportionally, therefore the correspondent voltage change is a measure of the acceleration by less than a constant of proportionality (Fig. 1-b). In the last decade experimental studies on the piezoresistance effect of SiNWs agreed that SiNWs under uniaxial stress offer an enhanced piezoresistance effect with respect to the bulk counterparts [2]-[6], [10]-[12].

The origin and behavior of this phenomenon called in the literature “Giant Piezoresistance”, is currently not clearly understood and research is at infancy stage. This effect would be of enormous impact on the performance of mechanical sensor. To date, relatively few reports on the development of silicon nanowire-based sensors are available [13], [14]. However, p-type single crystalline SiNWs have been studied for sensor applications [5], [10], [11], [15], [20].

Toriyama et al. [10] studied silicon nanowire piezoresistors fabricated by separation of implanted oxygen (SIMOX), thermal diffusion, electron beam (EB) direct writing, and reactive ion etching (RIE). In their study longitudinal and transverse piezoresistive coefficients, $\pi_{l\,<110>}$ and $\pi_{t\,<110>}$, were both dependant on the cross sectional area of the nanowires. The $\pi_{l\,<110>}$ of the nanowire piezoresistors increased (up to 60%) with a decrease in the cross sectional area, while $\pi_{t\,<110>}$ decreased with a increase in the aspect ratio of the cross section. The enhancement behavior of the $\pi_{l\,<110>}$ was explained qualitatively using 1-D hole transfer and hole conduction mass shift mechanisms. The reduction in the $\pi_{t\,<110>}$ with increase in the aspect ratio of the cross section is explained due to decreased stress transmission from the substrate to the nanowire. The

maximum value obtained of $\pi_{l\,<110>}$ of 48×10^{-11} Pa^{-1} at a surface concentration of 5×10^{19} cm^{-3}, indicate sufficient sensitivity for sensing applications.

Initial experimental studies undertaken by He and Yang [2] reported a very high piezoresistive effect (increased up to 3,776% with respect to the higher dimension counterparts) of self-assembled single crystal silicon nanowires in the <111> crystallographic orientation. Reck et al. [3] later used a lift-off and an electron beam lithography (EBL) technique to fabricate silicon test chips and studied the piezoresistive properties of crystalline and polycrystalline nanowires as a function of stress and temperature. They found that the piezoresistive effect in the <110> direction increased significantly as the silicon nanowire diameter decreased (up to 633%), consistent with the results from He and Yang [2]. Finally, Passi et al. [6] recently obtained an increase of piezoresistance of up to 2,140% respect to the bulk-Si in the same direction, the <110>.

To date, available published literature [2]-[4], [6], [17], agree that low doping and surface-to-volume ratio represent the main parameters that boost the piezoresistance effect of SiNWs. Some hypotheses have been speculated on the origin of such phenomenon. Recently the major culprit has been indicated to be surface-state induced effect for nanowires smaller than 70nm width, and enhanced strain modulation of carrier mobility for larger nanowires [4].

The use of silicon nanowires and yarns of carbon nanotubes as nanoscale piezoresistor **[**18**]** is a recent technology that may be embedded in the nano-electro-mechanical system (NEMS). Only few mechanical sensor prototypes that embed nanowires are available to date. A good example is that of Dao et al. [5], [12] who incorporated p-type silicon nanowires as piezoresistive elements in a miniaturized 3-degrees-of-freedom (3-DOF) accelerometer.

Roylance and Angell introduced the first fully integrated piezoresistive micromachined accelerometers in 1978 for biomedical applications [19], [20]. An excellent literature review of micromachined piezoresistive accelerometers was provided by Barlian et al. [14] and interested readers are referred to their paper. Today, accelerometers are heavily commercialized MEMS application. They are widely used in automotive (crash

detection and stability control), biomedical (activity monitoring), consumer electronics (portable computing, cameras lens stabilization, cellular phones), robotics (control and stability), structural health monitoring, and military applications.

Our paper presents the design and simulation of a novel single square millimeter 3-axial accelerometer for head injury g-loads detection for racecar drivers [21], [22], [25]. As accurate measuring of head accelerations is an important aspect in predicting head injury, it is important that the measuring sensor be well-coupled to the head [23]. Therefore, the main requirements of this application are miniaturization and high-G measurement range to allow the accelerometer incorporation into an earpiece. In order to fulfil these requirements nanowires as nanoscale piezoresistive devices have been chosen as sensing element, due to their high sensitivity and potential in miniaturization.

II. ACCELEROMETER DESIGN

Initial technical specifications have been specifically designed in order to address the particular application requirements (impact measurement) [24], see Table I. The device range measurement is for high-G impacts and the frequency response goes down to DC since head injuries may have long duration transient.

The mathematical modelling of the sensor is based on the classic mass-spring-damper mechanical system, see Fig. 1-a. The model of the sensing chip is shown in Fig. 2. The proof mass in the centre area is suspended by four surrounding beams that resemble springs, while the damper is air in the model. Each beam is clamped-clamped to the fix frame and the middle point is connected to the seismic mass. The overall geometric dimension of the chip is 1310 μm × 1310 μm × 400 μm. When acceleration is applied to the chip, the proof mass is displaced due to inertial force, resulting to beam deformation (Fig. 2).

The beam deformation, due to the applied stress (σ) (see Fig. 2), leads to a change in resistance (ΔR) of nanoscale piezoresistors proportional to the applied external inertial force (A). The fractional resistance

change in the measurement circuit is proportional to the output voltage drop as well, therefore representing a measure of the acceleration, as demonstrated in Fig. 1-b.

A. Finite Element Structural Analysis

The material selected for the mechanical structure of the sensing element is anisotropic single crystal silicon (SCS), which has been chosen for its mechanical properties (good stress tensile strength and high gage factor) [40]. The element used for the FE modelling is tetrahedron. The structure geometry, selected on sensitivity criteria, has been identified by an optimization process using commercially available software ANSYS 12.1. This process consisted of an extensive stress and modal analysis of tens of different geometries with the common feature of being highly-symmetric (i.e. symmetry on the principal X and Y-axes, the respective diagonals and rotating of multiple of 90°). These types of geometries allow the minimizing of the overall cross-sensitivity due to a self-cancelling feature.

Finite element modelling has been performed to verify mechanical behaviour of the structure and as well as to optimize the design. The optimization method uses an objective function which is to maximize the stress, using two constraints, the die size and the natural frequency. Fig. 3 and 4 show the optimization results of the mechanical structure under X- or Y-axis acceleration and Z-axis acceleration respectively. As it can be seen from the Figs. 3 and 4, all feasible points are below ~5 KHz, in order to get a bandwidth set in the specification of approximately 1 KHz (see section E for details). For all cases, under Z-axis and X- or Y-axis acceleration, the design points at higher equivalent stress has been selected as optimal designs.

The results of the optimization process are as follows: 1st mode shape (ω_{oz}) of 5,277.7 Hz, the maximum equivalent stress (σ_{eq}) at 250G acceleration in the X or Y-axis are 44.837 MPa and 66.041 MPa in the microscale and nanoscale piezoresistors respectively. In the Z-axis σ_{eq} at 250G acceleration is 66.581 MPa and 99.243 MPa in the microscale and nanoscale piezoresistors respectively.

By taking advantage of structure symmetry only the equivalent stress under X-axis acceleration as been analysed. The results for the Y-axis acceleration are equivalent.

Nanoscale piezoresistors, due to stress concentration region (i.e. the width is 10 times smaller than conventional piezoresistors), show an equivalent stress that is 47% higher than the conventional counterparts under 250G. This increase represents an initial sensitivity enhancement for geometrical reasons. Clearly progressively reducing the dimension will upraise the stress concentration effect. The 1st mode shape of the structure is a Z-axis bending at more than 5 kHz. This value defines the bandwidth of the device frequency response. Under an optimal damping design the upper frequency limit is of approximately 1 kHz, as set in the specifications.

B. Nanoscale Piezoresistor Arrangement

A total of 16 nanoscale piezoresistors were placed in strategic locations on the top surface of the mechanical structure (Fig. 5). Basically, in order to maximize the device electrical sensitivity, the piezoresistors were placed at the highest stress regions that were identified by FE stress distribution analysis.

A detailed image of a nanoscale piezoresistor placed in one of the chip corner is presented in Fig. 6. Each piezoresistor is geometrically identical with a length of 3 micrometer and a width of 100 nanometers.

C. Measurement Circuit

The measurement circuit is formed by three different full Wheatstone Bridges, one for each axis-sensing (Fig. 7).

Hence, the change in resistance of piezoresistors is measured as output voltage drop by these bridges. The advantage of using a bridge is that as the four resistors are identical, the effect of the temperature coefficient can be cancelled out by the balanced configuration. Moreover, the highly symmetric geometry chosen for the structure allows a self-cancellation of part of the cross-axis acceleration since the piezoresistors are intentionally positioned symmetrically.

There is a compensation effect related to acceleration on the X- and Y-axis. For X-axis acceleration the A_x-bridge becomes unbalanced and detects the acceleration on its output, while the A_y-bridge remains

balanced since, on each arm, one resistance decreases and the other one increases by the same quantity. Therefore, overall resistance on each arm remain unchanged. Simultaneously, the total resistance in the A_z-bridge remain unchanged since hypothetically, one resistance increases and the other one decreases by the same amount. This also gives a voltage drop of zero output since it remains balanced.

For Y-axis acceleration the A_y-bridge becomes unbalanced and detects the acceleration while the A_x-bridge remains balanced giving, theoretically, a differential output voltage (voltage drop) zero; therefore the cross-talk is nearly zero. The A_z-bridge, due to Y-axis acceleration behaves as follows, $R_{z1}+R_{z2}+R_{z3}+R_{z4}$ and $R_{z5}+R_{z6}+R_{z7}+R_{z8}$ remain unchanged, therefore the output remains zero.

Finally as in the case of Z-axis acceleration, the resistance decrement of A_x, A_y-bridge is theoretically equal since the geometrical symmetry of identically designed resistance, and the two bridges remain balanced at zero volt output. In contrast, the A_z-bridge, due to Z-axis acceleration becomes unbalanced and the output voltage is the measure of acceleration. Table II summarizes the values of the resistance change, + is an increment, - is a reduction and 0 unchanged.

In reality the 16 piezoresistors will not be of equal resistance and nor of perfect geometrical symmetry because of fabrication errors and non-linearity (as large deflection). Therefore some cross-talk on the output signal is expected in the calculated values for all bridges.

III. Performance

A. Electrical Sensitivity Analysis

The electrical sensitivity (S) of the accelerometer can be defined as the ratio between the output voltage and the applied acceleration. In case of in-plane acceleration (X or Y-axis), the longitudinal stress on the beams that are perpendicular to the direction of the applied acceleration is larger than that distributed on the beam which are parallel to the acceleration orientation. Therefore, the piezoresistors to measure A_x are arranged on the Y-oriented beams, and vice versa.

For example, in case of X-axis acceleration the electrical sensitivity for the A_x-bridge is as:

$$S_{A_x} = S_{A_y} = \frac{V_{out_{A_x}}}{A_x} = \frac{1}{A_x} \times \frac{\Delta R_x}{R_x} \times V_{in} \quad (1)$$

where V_{out} is the output voltage, V_{in} is the bias voltage applied to the piezoresistor and $\frac{\Delta R_x}{R_x}$ is the fractional resistance change of A_x Wheatstone bridge that is equal to:

$$\frac{\Delta R_x}{R_x} = \pi_l \cdot \sigma_l^y + \pi_t \cdot \left(\sigma_t^x + \sigma_t^z\right) \quad (2)$$

where π_l and π_t are longitudinal and transverse piezoresistive coefficient respectively. σ_l^y, σ_t^x, σ_t^z are respectively longitudinal stress in the Y-axis in case of acceleration along the X-axis, and transverse stress in the X and Z direction. The shearing stress is negligible and therefore neglected. It should be noted that the above equation is only valid for uniform stress fields or if the piezoresistor dimensions are small compared to the beam size [26].

Since the common approximation valid in the <110> direction, that is $\pi_l = -\pi_t$, the fractional resistance change becomes as:

$$\frac{\Delta R_x}{R_x} = \pi_l \cdot \left[\sigma_l^y - \left(\sigma_t^x + \sigma_t^z\right)\right] \quad (3)$$

The electrical sensitivity in the other directions is similarly calculated. The longitudinal piezoresistive coefficient at room temperature used for the conventional piezoresistor is 72×10^{-11} Pa^{-1} as reported by Smith [27] experimental work, while the correspondent nanoscale value, is of 1527×10^{-11} Pa^{-1}, obtained from Passi et al. [6] experimental work.

Temperature drift has been considered in the calculation (Temperature Coefficient of Sensitivity, TCS = 0.25%/°C) since the device is meant to be inserted inside the inner ear canal (~37°C). Therefore a further calculation of the sensitivity at the temperature of 37°C and 39.33°C has been undertaken, see Fig. 8. The latter temperature has been identified as the maximum temperature before a dermal injury of the ear skin occurs [28].

The temperature drift, as can be seen from Fig. 8, significantly reduces the sensitivity of the device. The linearity is not affected since the resistors are hypothetically identical and in a Wheatstone bridge configuration.

Table III summarizes the sensitivity change due to the temperature drift for the microscale piezoresistors. As can be seen on Table III the sensitivity is overall reduced of around 4% by an increment of almost 18 °C. This occurs because the increase of temperature reduces the value of piezoresistive coefficient corrected by the TCS. Similar results are obtained for the nanoscale piezoresistors.

However, the temperature drift calculated takes into account the piezoresistive coefficient variation only but ignore the variation of the resistance value, which is considered invariant, due to the small temperature range. Therefore if we consider the resistance temperature dependence overall the total effect is deteriorated.

The calculated electrical sensitivity of nanoscale piezoresistors in the <110> direction at low boron concentration at 37°C, increases of approximately 3,000% in comparison to the conventional ones, see Table IV.

Cross-sensitivity is below 5% for all axes due to the highly symmetric geometry selected, as discussed in the following section.

B. Cross-Axis Sensitivity Analysis

The cross-axis acceleration is an error of measurements related to different factors: the mechanical structure of the sensor and fabrication errors that affect its symmetry, the piezoresistors location on the top surface and the measurement circuit. Its sensitivity is calculated in percentage and it is the absolute value of

the fraction of the voltage output of each axis other than the one under stress and the axis under stress. For example the cross-axis sensitivities under the X-axis acceleration $S_{(Ax\text{-}Ay)\%}$ and $S_{(Ax\text{-}Az)\%}$ are detected respectively in the output of the A_y, A_z-bridge for the nanoscale piezoresistors as in (4) and (5):

$$S_{(Ax-Ay)\%} = S_{(Ay-Ax)\%} = \left| \frac{V_{out_{Ay}}}{V_{out_{Ax}}} \right| \% = 0.061\% \qquad (4)$$

$$S_{(Ax-Az)\%} = \left| \frac{V_{out_{Az}}}{V_{out_{Ax}}} \right| \% = 2.779\% \qquad (5)$$

As it can be seen the value obtained for Y-axis is the same as X-axis due to the geometrical symmetry. The cross-axis sensitivity related to the Z-axis acceleration is as follows:

$$S_{(Az-Ax)\%} = \left| \frac{V_{out_{Ax}}}{V_{out_{Az}}} \right| \% = 0.0058\% \qquad (6)$$

$$S_{(Az-Ay)\%} = \left| \frac{V_{out_{Ay}}}{V_{out_{Az}}} \right| \% = 0.0139\% \qquad (7)$$

Finally the calculated cross-axis sensitivity is less than 5% for all axes. These values are consequence of the highly symmetric geometry selected, the symmetric localizations of the piezoresistors on the top surface of the device and the measurement circuit (Fig. 5 and 7). Similar results are obtained for the microscale piezoresistors. In the next section the non-linearity is calculated.

C. Non-Linearity

The static response of the sensor (input/output relationship) is usually not perfectly linear. Non-linearities are mainly related to non-perfect ohmic contact of piezoresistors at high bias voltage (> 0.2V), and/or due to large deflection (structure stiffness changes). The former causes the I-V characteristic to become non linear, the latter is typically present for slender structures. Ohmic contact can be obtained by high boron doping concentration localized in the contact pad. Instead large deflection cannot be controlled in an open loop device. A controlled feedback is required (actuation) as in servo or force-balanced accelerometer. Typically the accelerometer that implements such system is the variable-capacitance accelerometer since the actuation is straightforward.

The easier solution for piezoresistive accelerometer is to correct this non-linearity electronically during calibration if necessary. A rule of thumb is that a large deflection occurs if the transverse displacements in a slender structure are more than 10% of the beam thickness. This last condition occurs in the proposed device approximately for acceleration over 100G and it has been taken into account in the FE analysis.

Due to the inherent linearity of the response obtained, the non-linearity is calculated using the End Point Linearity Method, instead of the more common Best Fit Straight Line Method (BFST) or Least Squares Best Fit Straight Line Method. This can be expressed as a percentage of either Full-Scale Output (FSO = 500G) or ± Full Scale (±FS = ±250G) in G's (G is the gravitational acceleration, i.e. = 9.8ms^{-2}).

The method for calculating the device non-linearity (*NL*) is [29]:

$$NL = \frac{\frac{MD}{S}}{FSO}\% = \%FSO \qquad (8)$$

The *NL* is calculated as the percentage of the fraction between the maximum deviation (*MD*) and the sensitivity (*S*) based on the *FSO* or *FS.* The result for both microscale and nanoscale piezoresistors is less than 1%FSO for all 3-axis.

D. Damping

Optimal damping design of the structure (damping ratio ζ = 0.7) offers the wider bandwidth in the amplitude-frequency relationship (flat dynamic response). Therefore, the gaps between top/bottom cup and proof mass of the accelerometer have been designed to work in this regime.

For vibration in the vertical direction (first mode shape), there are two main types of damping acting on the seismic mass, i.e. viscous damping and squeeze-film air damping. The latter occurs when the proof mass moves up and down, the air films trapped between the bottom/top surfaces of the seismic mass and the bottom/top caps are squeezed. This damping type is more dominant than the viscous damping. The damping ratio caused by double sided squeezed-film air damping is defined by (9), assuming that the air films have the same thickness d [30]:

$$\zeta = \frac{\beta \mu W^2}{H \rho g^3 \omega_{oz}} \rightarrow d = \sqrt[3]{\frac{\beta \mu W^2}{H \rho \zeta \omega_{oz}}} \qquad (9)$$

where β is correction factor depending on the ratio between the width W and the length of seismic mass, ρ is mass density of silicon (2,330 kg/m^3), μ is viscosity of the air (1.81×10^{-5} Pa-s), ω_{oz} is undamped natural radian frequency in the first shape mode (bending on Z-axis). For the proposed accelerometer, the value of d is found to be about 8.12 μm with optimal damping condition (ζ = 0.7).

Since this value endangers the beams performance for acceleration over 1,000G, bumpers are incorporated in the top/bottom cup (overload end stop in the Z-axis).

For the second and third mode shapes (rotation around X- or Y-axis), the gaps between the two side walls of the seismic mass and the two inner side walls of the frame have not been designed for an optimal damping. Priority has been given to the design of an optimized sensing chip structure (beam width). This gap is 50 μm. In this case, the squeezed-film air damping effect is much smaller than viscous damping. The damping ratio is therefore smaller than 0.7 (under-dumped), and optimal damping is not achieved.

E. Bandwidth

In this section, the usable frequency response of the proposed accelerometer is calculated which is defined as the flat area of its frequency response curve. To do this, it is necessary to know the behaviour of the spring mass damper model when it is added a harmonic force. A force of this type could, for example, be generated by a rotating imbalance. The applied sinusoidal acceleration with circular frequency ω is:

$$a = a_o \cdot \cos(\omega t) \tag{10}$$

The steady-state deflection of the spring is of the form:

$$x = x_o \cdot \cos(\omega t + \phi) \tag{11}$$

The deflection magnitude x_0 is related to the magnitude of the applied acceleration a_0 by:

$$x_o(\omega) = \frac{a_o}{(\omega_n)^2} \cdot \frac{1}{\sqrt{\left[1 - \left(\frac{\omega}{\omega_n}\right)^2\right]^2 + \left(2\zeta \frac{\omega}{\omega_n}\right)^2}} \tag{12}$$

As indicated by the notation, x_0 depends on the driving angular frequency (ω). In particular, x_0 becomes diminishingly small when ω is sufficiently large and the accelerometer will cease to be useful for accelerations at such a frequency. In practice, the useful bandwidth within which the accelerometer is used is given by the *upper cutoff frequency* ω_c. This frequency is the maximum frequency at which the relative amplitude remains constant and the accelerometer sensitivity remains uniform, it is defined conservatively by:

$$\frac{x_o(\omega_c)}{x_o(0)} = 1 \qquad (13)$$

and is given by

$$\omega_c = \gamma \cdot \omega_n \qquad (14)$$

where

$$\gamma = \sqrt{2\left(1 - 2\zeta^2\right)} \qquad (15)$$

In case of optimal damping ($\zeta = 0.7$) $\gamma = 0.2$ and the cut-off frequency, which determine the measurement bandwidth, is 1,055.54 Hz ($f_n = 5{,}277.7$ Hz), as set in the specification (Table I).

F. Noise

Noise is any output voltage that occurs when there is no acceleration applied to the sensor. There are three typical noise sources existing in all piezoresistive sensors, including the Johnson noise (noise floor or white noise), Hooge's noise (or 1/*f* noise, also called pink noise), and the thermo-mechanical noise (brown noise or Brownian noise).

Improvements in fabrication can drive the noise levels of the current piezoresistive accelerometer closer to the theoretical Johnson and Hooge asymptotes. Fig. 9 clearly shows the frequency dependence of noise in a piezoresistive accelerometer, with theoretical noise asymptotes also shown by Lynch et al. [31].

Johnson noise

Johnson noise is due to random motion (thermal agitation) of carriers in any electrical conductor. In a piezoresistor, Johnson noise can be described as [32]:

$$V_{Jn(rms)} = \sqrt{4K_B TR\Delta f} \qquad (16)$$

where K_B is Boltzmann's constant (1.38 × 10^{-23} J/K), T is temperature (37 °C), R is resistance of piezoresistor at low carrier density (1×10^{17}cm^{-3}), and Δf is the measurement bandwidth.
Accordingly, the calculated Johnson noises corresponding to nanoscale and microscale piezoresistors are shown on the Table IV.

Johnson noise does not depend on the frequency. The noise in the nanoscale piezoresistors is increased by around 200% due to one order of magnitude greater resistance than conventional microscale ones.

1/f noise

1/*f* noise is empirically determined noise, and can be estimated by [33], [41]:

$$V_{1/f(rms)} = \sqrt{\frac{\alpha V_{in}^2}{N} ln\left(\frac{f_{max}}{f_{min}}\right)\cdot\frac{1}{\Delta f}} \qquad (17)$$

where V_{in} is bias voltage across a piezoresistor with total number of carriers N; f_{max} and f_{min} are upper and lower limit of measurement frequency, respectively. α is a dimensionless parameter called Hooge parameter which, for an implanted resistor, has been found to vary depending on the anneal [34]. For a semiconductor, α was found to be 1e^{-7} [25], [35]. Several publications have shown that it is possible to decrease the value of α down to 3e^{-6} [34], [36]-[39].

For a constant doping concentration the number of carriers is calculated as $N = p \cdot l_p \cdot w_p \cdot t_p$, where p, l_p, w_p and t_p are, respectively, doping concentration, doping concentration length, width and depth of

piezoresistor. Because other noise sources are independent of the frequency range it is necessary to specify the 1/f noise for a specific bandwidth, this is done by dividing the 1/f noise by Δf.

Finally, the total $1/f$ noise voltage corresponding to each measurement bridge is calculated to be approximately 30 times greater in the nanoscale devices as clearly summarized on Table IV. This is mainly due to the very low carrier concentration.

Thermo-mechanial noise

Thermo-mechanical noise is the mechanical analog of Johnson noise, and consists of physical oscillations due to thermal agitation in the sensing structure. The thermo-mechanical noise equivalent acceleration can be written as [30]:

$$A_{TM} = \sqrt{\frac{8K_B T \omega_n \zeta}{m}} \qquad \left(\frac{m}{s^2} / \sqrt{Hz} \right) \qquad (18)$$

where m is the mass of the seismic mass and T is the surrounding temperature. The natural frequency for X or Y bending (mode 2 and 3) is: 5,539 Hz. The thermo-mechanical noise corresponding to each component of acceleration at 37 °C with the bandwidths mentioned above are in the order of few μg. $A_{TM}^{x,y}$ is the noise related to X and Y-axis and A_{TM}^{z} is the value related to Z-axis as described in (19) and (20).

$$A_{TM}^{x,y} = 25.7\,\mu g \qquad (19)$$

$$A_{TM}^{z} = 46.9\,\mu g \qquad (20)$$

Equivalent thermo-mechanical noise voltage can be obtained by applying (21) and (22):

$$V_{TM}^{x,y} = S_{A_{x,y}} \cdot A_{TM}^{x,y} = 20.9e^{-3} \cdot 25.7e^{-6} = 0.53\,\mu V \qquad (21)$$

$$V_{TM}^{z} = S_{Az} \cdot A_{TM}^{z} = 28.9e^{-3} \cdot 46.9e^{-6} = 1.35\,\mu V \qquad (22)$$

As can be seen in (18) the thermo-mechanical noise is inversely proportional to the square root of the mass. Therefore an increase of the mass can reduce the thermo-mechanical noise.

Total noise voltage

The total noise is calculated as the square root of the sum among the square power of each noise, as:

$$V_{Noise}^{Ax} = V_{Noise}^{Ay} = \sqrt{\left(V_{Jn}^{Ax}\right)^2 + \left(V_{1/f}^{Ax}\right)^2 + \left(V_{TM}^{x}\right)^2} \qquad (23)$$

Similar equation has been applied for the Z-axis.

Noise analysis indicates that the total voltage noise in the accelerometer is increased by 10 times in the X and Y-axis, and 4 times in the Z-axis, see Table IV.

The main contributor to the noise signal is the Hooge noise due to very low number of carriers in the nanoscale piezoresistors.

G. Resolution

The resolution of an accelerometer determines the minimum acceleration that can be measured. Resolution is defined as the noise divided by the sensitivity, therefore the resolution of the accelerometer is defined by (24) and (25):

$$R_{A_{x,y}} = \frac{V_{Noise}^{A_{x,y}}}{S_{Az}} \qquad (24)$$

$$R_{A_z} = \frac{V_{Noise}^{A_z}}{S_{Az}} \quad (25)$$

Table IV summerizes the sensor resolution calculated according to (24) and (25).

The resolution of the accelerometer with nanoscale piezoresistors is improved respect to the conventional microscale one of around 60-80% in all axes, due to their much higher sensitivity, see Table IV. However, the noise level of the nanoscale piezoresistors is worse than the conventional microscale ones because Johnson and Hooge noises are dependent on the resistance value and numbers of carriers respectively. Therefore, given the doping concentration, smaller size means higher resistance and lower number of carriers.

IV. DISCUSSION

The results obtained from the combined FE modeling, simulation of the mechanical structure and performance calculation of both MEMS and nanostructure are interesting for this field of study. Input values used as piezoresistive coefficient for calculating the sensitivity and cross-sensitivity are obtained from experiments of Passi [6] for the nanostructure and Smith [27] for the microstructure. This study raises the attention on silicon nanowires as devices being embedded into mechanical sensors as piezoresistors. The improved resolution of the designed accelerometer (less than 1mg on all axes) compared to the conventional ones with 60-80% increase (see Table IV) suggests that nanowires have the credential to be the sensing element of the future NEMS. This level of accuracy and precision of measurement is comparable to the capacitive counterparts' sensors.

To date only few laboratory prototypes have been fabricated, as reported by Dao et al. [12] suitable for low-G measurements. However, their device [12] sensitivity for each axis is only about 400 μVG^{-1}, and the resolution of 14 mg which requires further signal conditioning, see Table V.

Our work instead presents a sensor with higher sensitivity obtained by calculations (20.9 mVG^{-1}), mainly because a higher stress on the nanowires. This is thanks to the optimization process undertaken that

maximizes the stress on the beams of the mechanical structure, under the constraints specificied (see Table I). The resolution in this work is improved considerably compared to the work of Dao et al. [12] (see Table V) even if the sensor of Dao et al. is significantly smaller.

The performance calculated of the sensor met set sensor specifications. Cross-sensitivity, non-linearity and resolution are under the constraints set for this type of application, therefore the designed sensor results suitable for the bio-mechanical application of head injuries monitoring. Finally, the total noise of nanoscale piezoresistors results are much higher than the conventional ones, however, since in the nanoscale structures the sensitivity grows faster than the noise level, the overall resolution is significantly improved. It is worthwhile to point out that our work is based on previous published experimental works on nanowires structures used as piezoresistors. Experimental studies are currently underway and will be reported in the next future.

V. Conclusion and future work

This paper presents the design enhancement of a motion sensor for biomechanical measurement within a space-constrained environment. Due to the exploitation of electro-mechanical features of nanowires as nanoscale piezoresistors the nominal sensor sensitivity is overall boosted by more than 3,000%. This technology avoids the signal amplification but allows a higher resolution with the advantage of a smaller sensing element. Therefore, in comparison with conventional devices, the measured accuracy is considerably improved.

This achievement opens up new developments in the area of implanted devices where the high-level of miniaturization and sensitivity is often essential. Example applications are in hearing aid systems (implantable sound sensor for cochlear implants), heart wall motion measurement for cardiac artificial pacemakers and head injury monitoring, amongst others.

This study represents a valuable guideline for the development of future bio-motion sensing devices. The development of nanowires test-chips for design evaluation is ongoing at the moment. On-board car testing is planned next upon successful sensor fabrication and characterization.

ACKNOWLEDGEMENT

The authors are grateful for EPSRC funding support to M Messina under SEEDA EPSRC Case Award Voucher No.0900013338.

REFERENCES

[1] C. T. Huang, C. L. Hsin, K. W. Huang, C. Y. Lee, P. H. Yeh, U. S. Chen, and L. J. Chen, "Er-doped Silicon Nanowires with 1.54 um Light-emitting and Enhanced Electrical and Field Emission Properties," *Appl.Phys. Lett.*, 2007, vol. 91, issue 9, 093133

[2] R. He and P. Yang, "Giant piezoresistance effect in silicon nanowires," *Nature Nanotechnol.*, Oct. 2006, vol. 1, issue 1, pp. 42–46.

[3] K. Reck, J. Richter, O. Hansen, and E. V. Thomsen, "Piezoresistive effect in top-down fabricated silicon nanowires," in *MEMS 2008. IEEE 21st International Conference on Micro Electro Mechanical Systems*, 2008, pp. 717–720.

[4] T. Barwicz, L. Klein, S. J. Koester and H. Hamann, "Silicon nanowire piezoresistance: Impact of surface crystallographic Orientation," *Appl. Phys. Lett* , 2010, vol. 97, issue 2.

[5] D. V. Dao, K. Nakamura, T. T. Bui and S. Sugiyama, "Micro/nano-mechanical sensors and actuators based on SOI-MEMS technology," *Adv. in Nat. Sciences: Nanoscience and Nanotechnology*, 2010.

[6] V. Passi, F. Ravaux, E. Dubois, J.-P. Raskin , "Backgate bias and stress level impact on giant piezoresistance effect in Thin silicon films and nanowires," in *IEEE MEMS 2010*, 2010, pp. 464 – 467.

[7] M. L. Lee, E. A. Fitzgerald, M. T. Bulsara, M. T. Currie and A. Lochtefeld, "Strained Si, SiGe and Ge channels for high-mobility metal-oxide–semiconductor field-effect transistors," *J. Appl. Phys.,* Jan. 2005, vol. 97, issue 1, pp. 011101 -1.

[8] B. M. Haugerud, L. A. Bosworth and R. E. Belford, "Mechanically induced strain enhancement of metal-oxide–semiconductor field-effect transistors," *J. Appl. Phys*., 2003, vol. 94, issue 6, pp. 4102–4107.

[9] L. J. Chen, "Silicon nanowires: the key building block for future electronic devices," *J. of Mat. Chem.*, 2007, vol. 17, issue 44, 4639–4643.

[10]T. Toriyama, Y. Tanimoto, and S. Sugiyama, "Single crystal silicon nano-wire piezoresistors for mechanical sensors," *J. Microelectromech. Syst.*, 2002, vol. 11, issue 5, pp. 605–611.

[11]T. Toriyama, D. Funai, and S. Sugiyama, "Piezoresistance measurement on single crystal silicon nanowires," *J. of Appl. Phys.*, 2003, vol. 93, issue 1, pp. 561–565.

[12]D. V. Dao, T. Toriyama, and S. Sugiyama, "Noise and frequency analyses of a miniaturized 3-DOF accelerometer utilizing silicon nanowire piezoresistors," in *Proc. of IEEE, Sensors 2004*, vol. 3, pp. 1464–1467.

[13]M.-W. Shao, Y.-Y. Shan, N.-B. Wong, and S.-T. Lee, "Silicon Nanowire sensors for bioanalytical applications: Glucose and hydrogen peroxide detection," *Adv. Funct. Mat.*, Sep. 2005, vol. 15, isuue 9, pp. 1478–1482.

[14]A. A. Barlian, W.-T. Park, J. R. Jr. Mallon, A. J. Rastegar, and B. L. Pruitt, "Review: Semiconductor Piezoresistance for Microsystems," in *Proc. of the IEEE,* 2009, vol. 97, n. 3.

[15]A. Okamura, D. V. Dao, T. Toriyama and S. Sugiyama, "Fabrication of an Ultra Small Accelerometer Utilizing Si Nanowire Piezoresistors," *in Proc. of the 22nd Sensor Symposium*, 2005, pp. 203-206.

[16]A. Sakai, D. V. Dao, A. Okamura, S. Sugiyama, "Fabrication of an Ultra Small 3-DOF Accelerometer Utilizing Small External Influence Structure and Si Nanoscale Piezoresistors," *in Proc. of the 23rd Sensor Symposium*, 2006, pp. 270-273.

[17]K. Nakamura, Y. Isono, and T. Toriyama, “First-Principles Study on Piezoresistance Effect in Silicon Nanowires,” *Jap. J. of Appl. Phys.*, Jun. 2008, vol. 47, No. 6, pp. 5132–5138.

[18]T. Mirfakhrai, J. Oh, M. E. Kozlov, S. Fang, M. Zhang, R. H. Baughman, and J. D. W. Madden, “Mechanoelectrical Force Sensors Using Twisted Yarns of Carbon Nanotubes“ *IEEE/ASME Trans. On Mechatronics*, Vol. 16, No. 1, Feb. 2011.

[19]L. M. Roylance, ‘‘A miniature integrated circuit accelerometer for biomedical applications,’’ Ph.D., Electrical Engineering Department, Stanford University, 1978.

[20]L. M. Roylance and J. Angell, ‘‘A Batch-fabricated silicon accelerometer,’’ *IEEE Trans. Electron Devices*, vol. 26, issue 12, pp. 1911–1917, Dec. 1979.

[21]Olvey Stephen E., Knox Ted, Cohn Kelly A., “The development of a method to measure head acceleration and motion in high-impact crashes”, *Neurosurgery,* vol. 54, pp. 672-677, 2004.

[22]E. Nassiopoulos and J. Njuguna, “An assessment of the side impact protection systems (SIPS) for racing drivers in motorsport rallying championships,” unpublished.

[23]T. Knox, “Validation of earplug accelerometers as a means of measuring head motion,” presented at the 2004 SAE Motorsport engineering Conference and Exhibition, Dearborn, Mi. SAE 2004-01-3538.

[24]J. S. Wilson and Knovel, *Sensor technology handbook*, Elsevier, Amsterdam; Boston, 2005.

[25]M. Unser, “Motorsports Accidentology”, MSc thesis, School of Applied Sciences, Cranfield University, Cranfield, UK, 2009.

[26]R. Amarasinghe, D.V. Dao, V.T. Dau, B.T. Tung.and S. Sugiyama, “Sensitivity Enhancement Of Piezoresistive Micro Acceleration Sensors With Nanometer Stress Concentration Regions On Sensing Elements,” presented at the Transducers 2009, Denver, CO, USA, 2009, June 21-25.

[27]C. S. Smith, “Piezoresistance effect in germanium and silicon,” *Phys. Rev.*, vol. 94, issue 1, pp. 42-49, Apr. 1954.

[28]ASTM C1055 - 03(2009), Standard Guide for Heated System Surface Conditions That Produce Contact Burn Injuries, available at: http://www.exponent.com/scalds_burn_injuries/.

[29]Freescale Semiconductor , Accelerometer Terminology Guide, 2007. Available: http://cache.freescale.com/files/sensors/doc/support_info/SENSORTERMSPG.pdf

[30]S. Middelhoek, "Micro mechanical transducers", in *Handbook of sensors and actuator,* M. -H. Bao ed., Elsevier, 2000.

[31]J. P. Lynch, A. Partridge, K. H. Law, T. W. Kenny, A. S. Kiremidjian, and E. Carryer , "Design of Piezoresistive MEMS-Based Accelerometer for Integration with Wireless Sensing Unit for Structural Monitoring," *J. of Aerospace Engineering*, vol. 16, issue 3, pp. 108-114, 2003.

[32]H. Nyquist, "Thermal agitation of electric charge in conductors," *Phys. Rev.,* vol. 32, pp. 110-113, 1928.

[33]J. A. Harley and T. W. Kenny, "1/f noise considerations for the design and process optimization of piezoresistive cantilevers," *J. Microelectromechan. Syst.*, vol. 9, pp. 226-235, 2000.

[34]L. K. J. Vandamme and S. Oosterhoff , "Annealing of ion-implanted resistors reduces the 1/f noise," *J. Appl. Phys.,* vol. 59, pp. 1-74, 1986.

[35]L. K. J. Vandamme, "Is the 1/f noise constant? ," in *Noise in Physical Systems and 1/f noise,* Elsevier, Amsterdam, 1983, pp. 183-192.

[36]H. Chen, M. Bao, H. Zhu, S. Shen, "A piezoresistive accelerometer with a novel vertical beam structure," *J Sens Actuators Phys*, vol. 63, pp. 19-25, 1997.

[37]M. Tacano, J. Pavelka, N. Tanuma, S. Yokokura, S. Hashiguchi, "Dependence of Hooge constant on mean free paths of materials," in *Proc. SPIE,* 2004, vol. 5469, pp. 310-319.

[38]P. Gonzales, S. Severi, S. Lenci, P. Merken, A. Witvrouw, K. D. Meyer, "Evaluation of piezoresistivity and 1/f noise of polycrystalline SiGe for MEMS sensor application," in *Proc. Eurosens XXII,* 2008, pp. 881.

[39]J. A. Harley, "Advances in piezoresistive probes for atomic force microscopy," PhD dissertation thesis, Stanford University, 2002.

[40]N. Maluf , *An Introduction to Microelectromechanical Systems Engineering*, 2nd ed. Boston: Arttech House, 2004.

[41]F. N. Hooge, "1/f noise is no surface effect," *Physical letters A,* vol. 29, pp. 139-140, 1960.

Caption of Figures and Tables

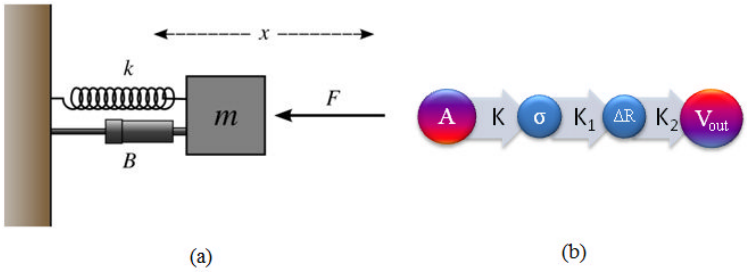

Figure 1. (a) Mass-spring-damper mechanical system; (b) Graphical representation of the electro-mechanical physic involved in the sensing (K, K_1, K_2 are constants).

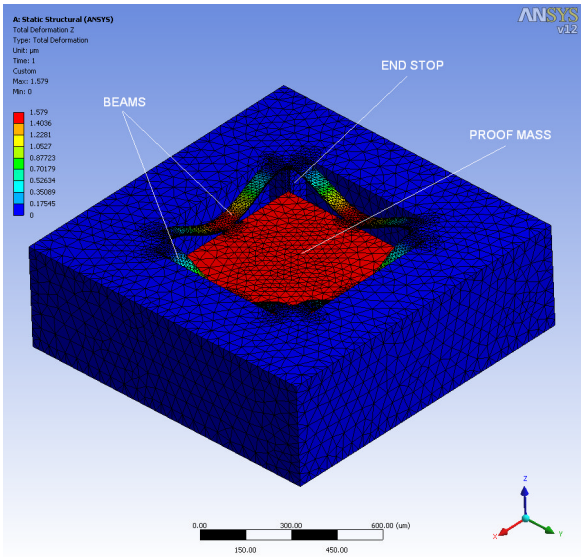

Figure 2. Model of the accelerometer under stress due to external forces. The red color corresponds to the maximum displacement of the proof mass. In blue is the surrounding frame which remains undeformed. As it can be seen the beams change color gradually from blue to red due to deformation.

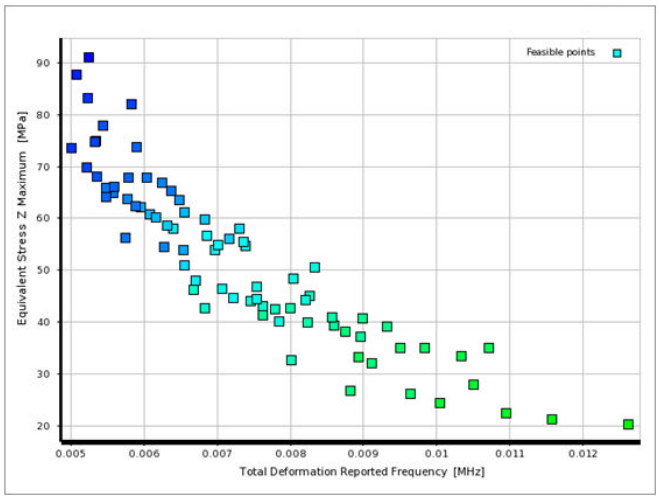

Figure 3. Design optimisation results under Z-axis acceleration. Maximum equivalent stress on Y-axis and natural frequency on the X-axis. All points below 5 KHz are feasible design points.

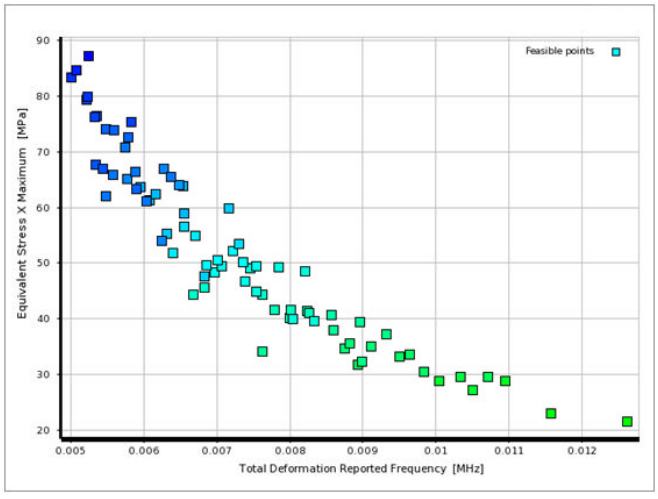

Figure 4. Design optimisation results under X-axis acceleration. Similar results were obtained for Y-axis acceleration.

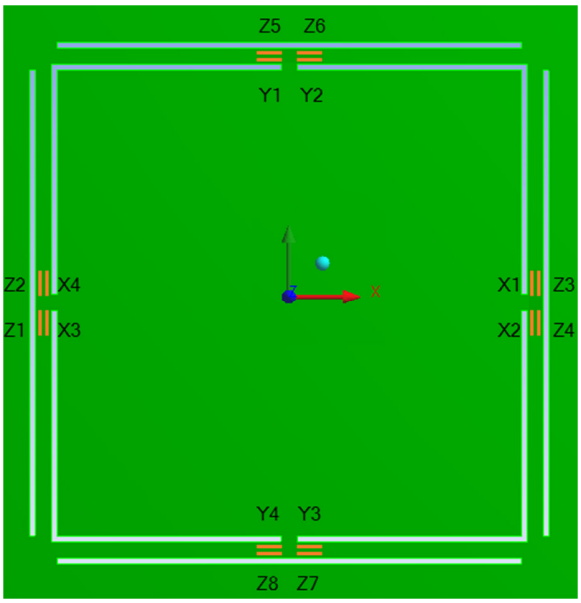

Figure 5. Piezoresistors location. 16 nanoscale piezoresistors, in orange, are placed in strategic location where is present the maximum stress in order to maximize the sensitivity and minimize the cross-sensitivity (top view)

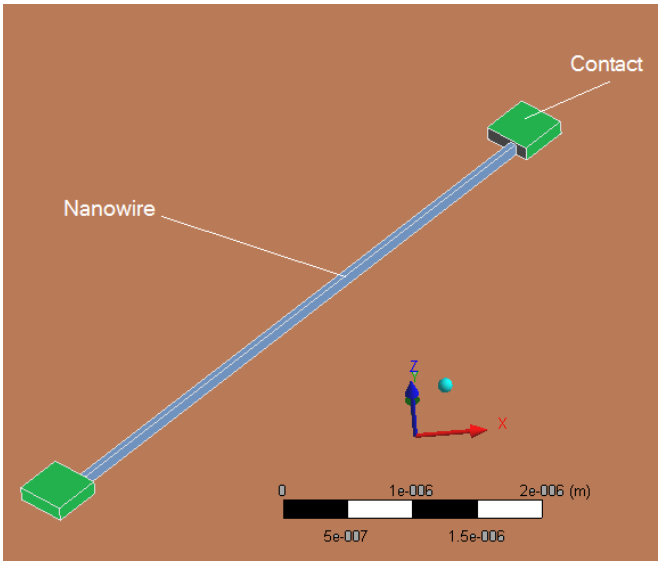

Figure 6. Nanoscale piezoresistor model

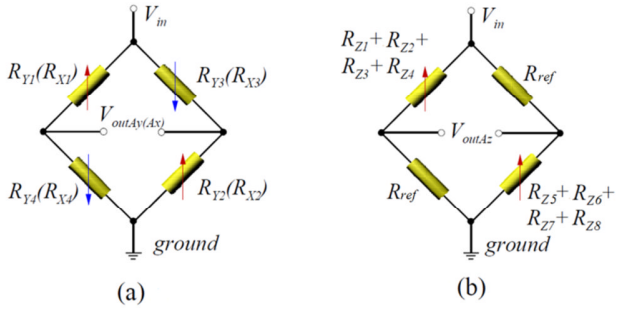

Figure 7. (a) A_x-, A_y-bridge and (b) A_z- Wheatstone Bridge measurement circuit

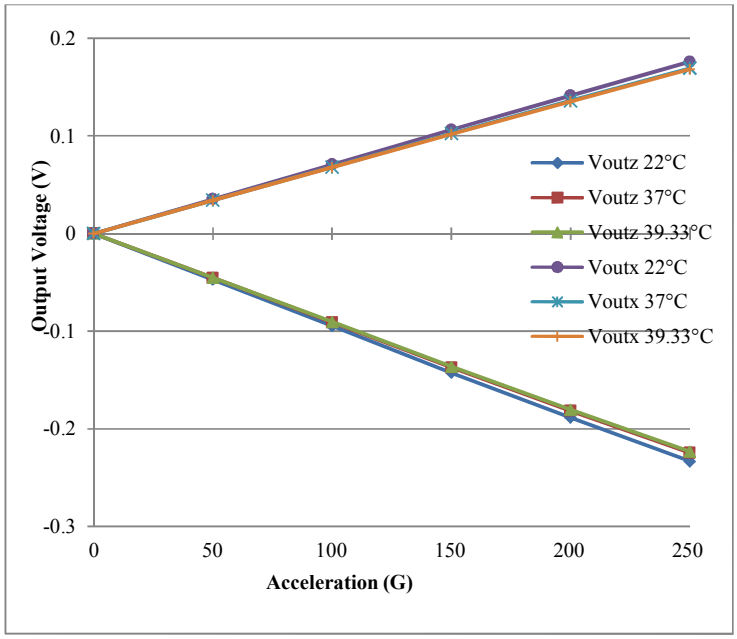

Figure 8. Temperature drift – Output voltage vs. X- or Y-axis and Z-axis acceleration. It was observed that the sensitivity is progressively reduced due to temperature increase.

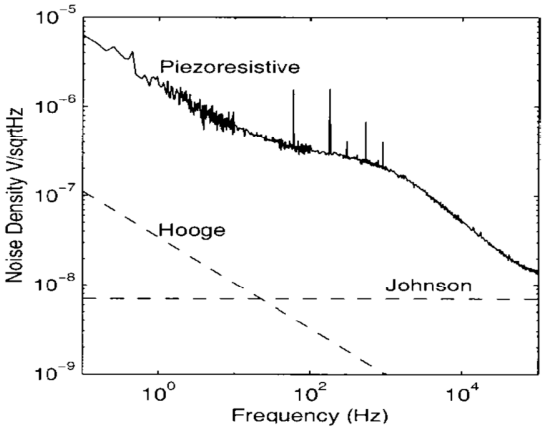

Figure 9. Noise spectral density of piezoresistive accelerometer illustrating the combined Hooge and Johnson noise [31]

TABLE I. SENSOR TECHNICAL SPECIFICATIONS

Range	±250 G
Sensitivity	4 mV/G
Frequency response	0 to 1,000 Hz
Shock limit	±1,000 G
Resolution	<10 mG
Non-Linearity	<1% FSO
Cross-Sensitivity	<5%
Dimension	<2×2×1 mm^3

TABLE II. RESISTANCE CHANGE

	R_{x1}	R_{x2}	R_{x3}	R_{x4}	R_{y1}	R_{y2}	R_{y3}	R_{y4}	$R_{z1}+R_{z2}+R_{z3}+R_{z4}$	R_z
$\mathbf{A_x}$	-	-	+	+	+	-	-	+	0	
$\mathbf{A_y}$	-	+	+	-	-	-	+	+	0	
$\mathbf{A_z}$	-	-	-	-	-	-	-	-	-	

TABLE III. TEMPERATURE DRIFT – SENSITIVITY

Temperature (°C)	***Ax*, *Ay* (mV/g)**	***Az* (mV/g)**
22	0.684	0.907
37	0.677	0.898
39.33	0.655	0.868

TABLE IV. VOLTAGE NOISE – SENSITIVITY – RESOLUTION

	Microscale		***Nanoscale***	
	Ax*, *Ay	***Az***	***Ax*, *Ay***	***Az***
V_{jn} **(µV)**	1.01	1.42	3.2	4.52
$V_{1/f}$ **(µV)**	0.4	0.28	13.14	9.29
V_{Noise} **(µV)**	1.2	1.97	13.53	10.41
***Sensitivity* (mV/g)**	0.677	0.898	20.9	28.9
***Resolution* (mg)**	1.78	2.2	0.64	0.36

TABLE V. SENSOR COMPARISON

	Microscale		***Nanoscale***	
	Present work	**Dao et al. [5]**	**Present work**	**Dao et al. [12]**
Range	High-G	Low-G	High-G	Low-G
Sensitivity **(μV/g)**	677	30	20,900	400
Resolution **(mg)**	1.78	-	0.64	14
Cross-Sensitivity ***(%)***	2.78	5.5	2.78	-
Dimension **(mm^3)**	1.3×1.3×0.4	1×1×0.45	1.3×1.3×0.4	0.5×0.5×0.35